AIAA 80-0184R

Flowfield about and Forces on Slender Bodies at High Angles of Attack

William J. Yanta* and Andrew B. Wardlaw Jr.*
Naval Surface Weapons Center, Silver Spring, Md.

A rigidly supported tangent ogive model has been tested in low-turbulence, incompressible flow at incidences of 25, 35, 45, and 55 deg. A constant crossflow Reynolds number of 1×10^5 was maintained which produced laminar boundary-layer separation. Both unsteady surface pressures and flowfield velocities were measured, the latter with a three-component Laser Doppler Velocimeter. Analysis of the results indicates that high levels of velocity and surface pressure fluctuations occur downstream of the nose on the leeside of the model. An analysis of mean pressure and velocity distributions indicates that the maximum local side force occurs as the first vortex is shed and is directed toward the side with the remaining vortex. Far from the nose the flowfield shows reduced vorticity peaks and a disappearance of highly asymmetric pressure distributions. The portion of the flowfield causing peak side forces is concluded to be predominantly steady and varying side force levels are produced by changes in the mean vortex pattern.

Nomenclature

C_{dc}	$=F_N/(Dq\sin^2\alpha)$
C_p	= average value of $(p-p_\infty)/(q\sin^2\alpha)$
Cy	$=Fy/(Dq\sin^2\alpha)$
D	= model diameter (5.67 cm)
F_N	= normal force per unit length
Fy	= side force per unit length
q	= freestream dynamic pressure
Re, Re_c, Re_s	= Reynolds number based on freestream properties and D, $D\sin\alpha$, and $D/\sin\alpha$, respectively
U_∞	= freestream velocity
u, v, w	= Cartesian velocity components
$\bar{u}, \bar{v}, \bar{w}$	= average velocity component value
x, y, z	= Cartesian coordinates (see Fig. 1)
x'	= distance along model axis measured from nose tip
z'	= distance in the z direction measured from model axis
z''	= distance in the z direction measured from rear stagnation point
α	= angle of attack
Γ	= circulation, m^2/s
σ	= standard deviation
ϕ	= circumferential angle (windward is at $\phi=0$ deg)
ω	= [Γ/unit area] $D/(\pi U_\infty \sin\alpha)$

I. Introduction

INCREASED performance requirements have made it necessary for missiles to fly at large angles of attack. At incidences greater than a few degrees, the flow separates from the leeside of the body, rolling up to form a pair of symmetric vortices. With increasing angle of attack the shed vortices form a nominally steady and asymmetric pattern, even on axisymmetric bodies. In subsonic and transonic flow, these vortices have a dominant and nonlinear influence on vehicle aerodynamics. Engineering methods for estimating aerodynamic coefficients are empirical or semiempirical in nature and rely on force measurements, surface pressure data, or an experimental description of the high-angle-of-attack flowfield. Unfortunately, lack of repeatability has plagued high-incidence testing in these speed regimes and it has not been possible experimentally to define quantitatively the flowfield, surface pressure distributions, or aerodynamic coefficients. Most strongly affected is the degree of asymmetry in the pressure distribution and the resulting yaw plane loads. Both of these quantities vary with changes in the roll orientation of axisymmetric models.

The low-speed flow visualization studies of Clark[1] and Clark and Nelson[2] suggest that the high-angle-of-attack flowfield is dominated by two clearly defined nose vortices. The coherence of subsequent vortices decreases with increasing distance from the nose and only the first three or four vortices, at most, are distinguishable. Upstream of the axial station where vortices are shed, the vortex pattern is relatively steady. However, the point of vortex shedding seems to jump randomly in time between several well-defined locations which results in various asymmetric patterns and possible switching from a symmetric to an asymmetric vortex pattern. In other studies very small changes in test conditions have been observed to produce different asymmetric vortex patterns.[3,4] Differential pressure measurements suggest that vortex patterns may jump to the mirror image state.[5]

Side force has been observed to be distributed sinusoidally along the length of an inclined circular body.[5,6] The peak closest to the nose is the largest and successive ones are progressively smaller, with side force disappearing altogether after several cycles. The regions of the body experiencing large side loads are approximately those near which Clark[1] has observed well-defined vortex structures. The disappearance of side force at large distances from the nose is presumably caused by amorphous vortices in this area.

Past research on side force and moment has not resolved the reason for nonrepeatability of side force measurements. Side force is a product of coherent, asymmetric leeside vortices which have been observed to be unsteady principally downstream of the shedding points. However, it is not clear which portion of the vortex pattern induces side force and whether this part of the pattern is predominantly steady or unsteady. If the region of the flowfield causing large side loads is steady, side force nonrepeatability is probably caused by variations in the average vortex pattern triggered by small changes in the test conditions and model anomalies on the order of machining tolerances. Alternatively, Lamont and Hunt have presumed that unsteadiness is the principal cause of nonrepeatability. They theorize that freestream turbulence

Presented as Paper 80-0184 at the AIAA 18th Aerospace Sciences Meeting, Pasadena, Calif., Jan. 14-16, 1980; submitted Feb. 7, 1980; revision received Oct. 21, 1980. This paper is declared a work of the U. S. Government and therefore is in the public domain.

*Aerospace Engineer. Member AIAA.

induces random changes in the vortex pattern which can be idealized as switching to a mirror-image configuration.[5,6]

A large number of experimental studies of the high-angle-of-attack flowfield are documented in the literature covering a broad range of Mach and Reynolds numbers.[7-18] The current work is unique in that pressure data were taken in conjunction with the velocity measurements, a method which allows the coupling between flowfield structure and surface pressure profiles to be determined. Tests were conducted in low-speed flow under conditions which featured laminar separation of the boundary layer. In order to minimize repeatability problems, the tests were carried out on a rigidly mounted model in a relatively low-turbulence environment (0.1%).

A description of the experiment is provided in Sec. II, while the steady and unsteady results are reported in Sec. III. Section IV features a discussion of the results and the more salient conclusions are summarized in Sec. V. A more detailed description of the current work can be found in Ref. 19.

II. Description of the Model and Experiment

The experimental model, shown in Fig. 1, was a 5.67 cm diam tangent ogive with a nose fineness of 3 and afterbody length of 9.6 calibers. Six cross-sectional stations were each instrumented with 24 pressure taps located circumferentially at intervals of 15 deg. Pressures were monitored using three internally mounted ±0.69 kPa (±0.1 psi) Setra differential pressure transducers. Each of these devices was connected to a 48 port internally mounted scanivalve allowing all 144 pressure taps to be sampled. In order to maximize the response of the pressure-measuring system the lengths of the tubes connecting pressure taps to the scanivalves were minimized. Pretest calibrations indicated that pressure fluctuations on the order of 500 Hz could be measured. A recently developed three-component Laser Doppler Velocimeter (LDV), described in Ref. 20, was used to survey the leeward flowfield structure. As shown in Fig. 1, survey planes were perpendicular to the freestream direction.

The experiment was carried out in a low-speed, closed-circuit wind tunnel at an Re_c of 1×10^5 (i.e., $U_\infty \sim 25/\sin\alpha$ m/s) and at incidences of 25, 35, 45, and 55 deg. Pretest hot-wire anemometer calibrations of the test section indicated an ambient turbulence level (i.e., u'/U_∞) of 0.1% for the streamwise velocity component. The actual procedure for acquiring data was as follows:

1) The LDV system was focused on a specific point in the flowfield and each of the three pressure transducers was positioned to a selected surface pressure tap.

2) A velocity and pressure data point was recorded whenever a valid measurement of each of the three velocity components was acquired within a 100 μs time window.

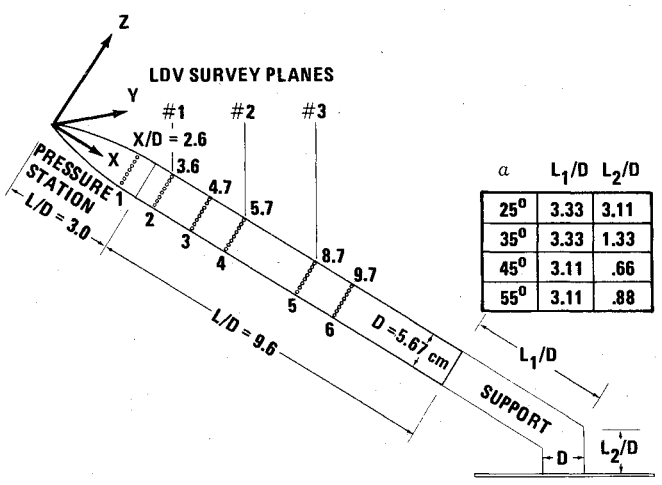

Fig. 1 Tangent ogive pressure model and support system (rows of small circles indicate locations of pressure measuring stations).

3) With the LDV focused at the same point in the flowfield and the pressure transducers positioned at the same surface pressure taps, step 2 was repeated until 200 data points had been taken, which generally took less than a minute.

4) The focus point of the LDV system was then changed and the scanivalves were rotated to connect another set of three surface pressure taps. The above procedure was then repeated until the entire traverse plane had been mapped.

A sufficient number of flowfield points were probed during each run to complete a map of a single traverse plane. On the forward plane about 100 points were measured, while on the aft plane the necessary number increased to nearly 200. Three separate runs were required at each incidence to map all three traverse planes and each provided a complete set of surface pressure data. The same model roll angle was maintained throughout the entire test series.

The above experimental procedure allowed determination of mean velocity, mean surface pressures, and the standard deviation of these quantities using the sample of 200 data points taken at each location.

Repeated visits to the same pressure taps increased the number of samples available for the analysis of pressure data. Recording of the data was triggered by the acquisition of a valid measurement for each of the velocity components. Since this occurred at random intervals in time and the time at which each sample was taken was not measured, spectral analysis of the results was not possible.

III. Experimental Results

Condition of the Boundary Layer

The condition of the separating boundary layer can be determined by examining the circumferential pressure profile. Data at the aftmost pressure station for an incidence of 25 deg are illustrated in Fig. 2. Also shown are the typical laminar and turbulent separation profiles measured by Bursnall and Loftin[21] on an infinite inclined cylinder at an incidence of 30 deg. The present results are qualitatively similar to the laminar separation data, indicating that laminar separation occurred during the present study.

Velocity and Pressure Fluctuations

Using the data generated in the current study it is possible to determine the standard deviation σ as well as the mean value of both velocity and pressure. The large values of σ encountered in this study are greatly in excess of the background noise and reflect occurrences in the flowfield.

Typical flowfield distributions of σ_u and σ_w values, normalized by the freestream velocity, are shown using contour plots in Fig. 3. The illustrated data were taken on traverse plane 3 at incidences of 25 and 55 deg. The channel on which the v velocity data were recorded was excessively noisy due to instrumentation problems. Although this did not seriously degrade the estimated average values, σ_v is not reflective of the flowfield and will not be discussed.

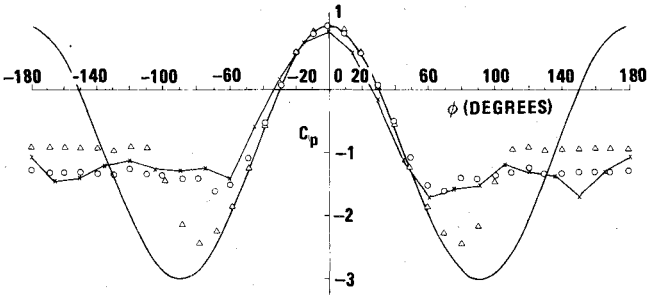

Fig. 2 Aft station pressure measurements compared to the yawed cylinder data of Bursnall and Loftin[21] ——potential flow, x——x tangent ogive data at $\alpha = 25$ deg, ○ laminar yawed cylinder data at $\alpha = 30$ deg. Δ turbulent yawed cylinder data at $\alpha = 30$ deg.

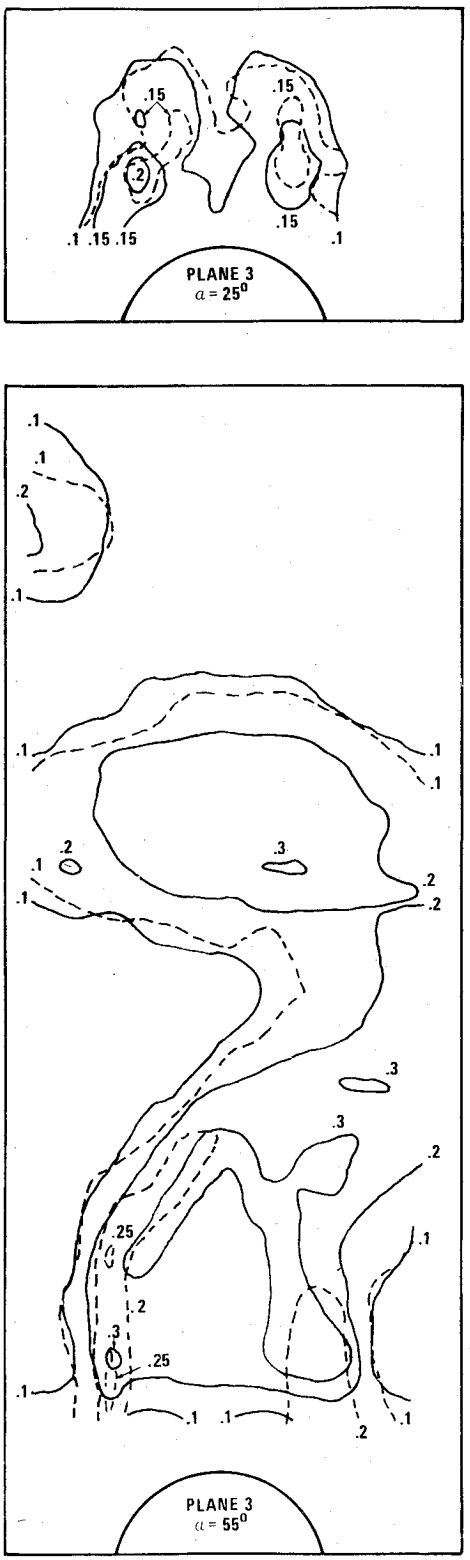

Fig. 3 Contour maps of u and w component fluctuations (——σ_w/U_∞;- - - -σ_u/U_∞).

An examination of Fig. 3 indicates that peak σ_w values exceed those of σ_u and do not necessarily occur at the same location. The peak values of both components are coincident with regions where high vorticity is expected and appear also to cover the feeding sheet area. An examination of data from all three traverse planes indicates that the region of the flowfield experiencing large velocity fluctuations increases with increasing distance from the nose. However, peak σ_u and σ_w values in the aft plane were only slightly higher than those

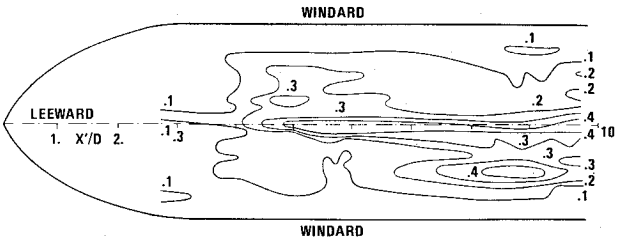

Fig. 4 Contour of σ_{C_p} values at incidence of 45 deg.

on the foremost plane in most cases and remain unchanged in a few.

The large fluctuations in flowfield velocities apparently induce a high level of surface pressure variation. A contour plot of σ_{C_p} values over the model surface is shown in Fig. 4 for an incidence of 45 deg. High levels of σ_{C_p} are found principally on the leeside of the model with peak values occurring at distances greater than 5-6 caliber from the nose tip. On the ogive itself, σ_{C_p} values are relatively low even on the leeside. With increasing angle of attack the zone featuring large values of σ_{C_p} expands circumferentially and peak values increase, reaching a maximum at $\alpha = 45$ deg in the current test series. These changes may have been partly affected by variations in Re_∞ with angle of attack.

Description of the Flowfield and Surface Pressure Distribution

The distribution of vorticity throughout the flowfield can be calculated by dividing the surveyed portion of the traversed plane into quadrilateral elements with the corners located at points where flowfield velocities were measured. The circulation associated with each element is calculated using:

$$\Gamma = \oint v\,\overline{ds} = \tfrac{1}{2}\{\bar{n}_{12}(\bar{v}_1 + \bar{v}_2) + \bar{n}_{23}(\bar{v}_2 + \bar{v}_3) + \bar{n}_{34}(\bar{v}_3 + \bar{v}_4) + \bar{n}_{41}(\bar{v}_4 + \bar{v}_1)\} \quad (1)$$

Here $\bar{n}_{ij}$ is the vector connecting element corners i and j while $\bar{v}_i$ is the velocity vector at corner i. The resulting circulation is assigned the location of the element centroid.

Contour maps showing the vorticity distribution throughout the flowfield are constructed using the values of vorticity from Eq. (1). Results for all three of the traverse planes are shown in Figs. 5 and 6 for the incidences of 45 and 55 deg, respectively, which featured highly asymmetric flowfields. Also provided are C_p and σ_{C_p} profiles at each of the adjacent pressure stations and the σ_w distribution in each of the mapped traverse planes. The displayed C_p and σ_{C_p} data were taken during the same run in which the flowfield was probed.

An examination of Figs. 5 and 6 produces the following description of the development of the flowfield, pressure distribution, and side force along the length of the tangent ogive model. At low incidences and near the model nose, vortices develop symmetrically producing symmetric C_p and σ_{C_p} distributions. A high level of velocity fluctuation occurs in those regions of the flowfield which feature large values of vorticity. With increasing incidence and distance from the model nose, one of the vortices moves away from the leeside of the model. The estimated total strength of the shed vortex is consistently greater than that of its companion. As the first vortex starts to move away from the model, the remaining vortex appears to rotate toward the leeside. The pressure distribution now becomes highly skewed and the maximum side force occurs. The direction of this force is toward the side featuring the remaining vortex and is a result of the large suction peak induced by this structure. The σ_{C_p} distribution which was approximately symmetric prior to the shedding of the first vortex now becomes highly skewed with higher values occurring on the side with the closer vortex. With increasing distance from the model nose (i.e., see

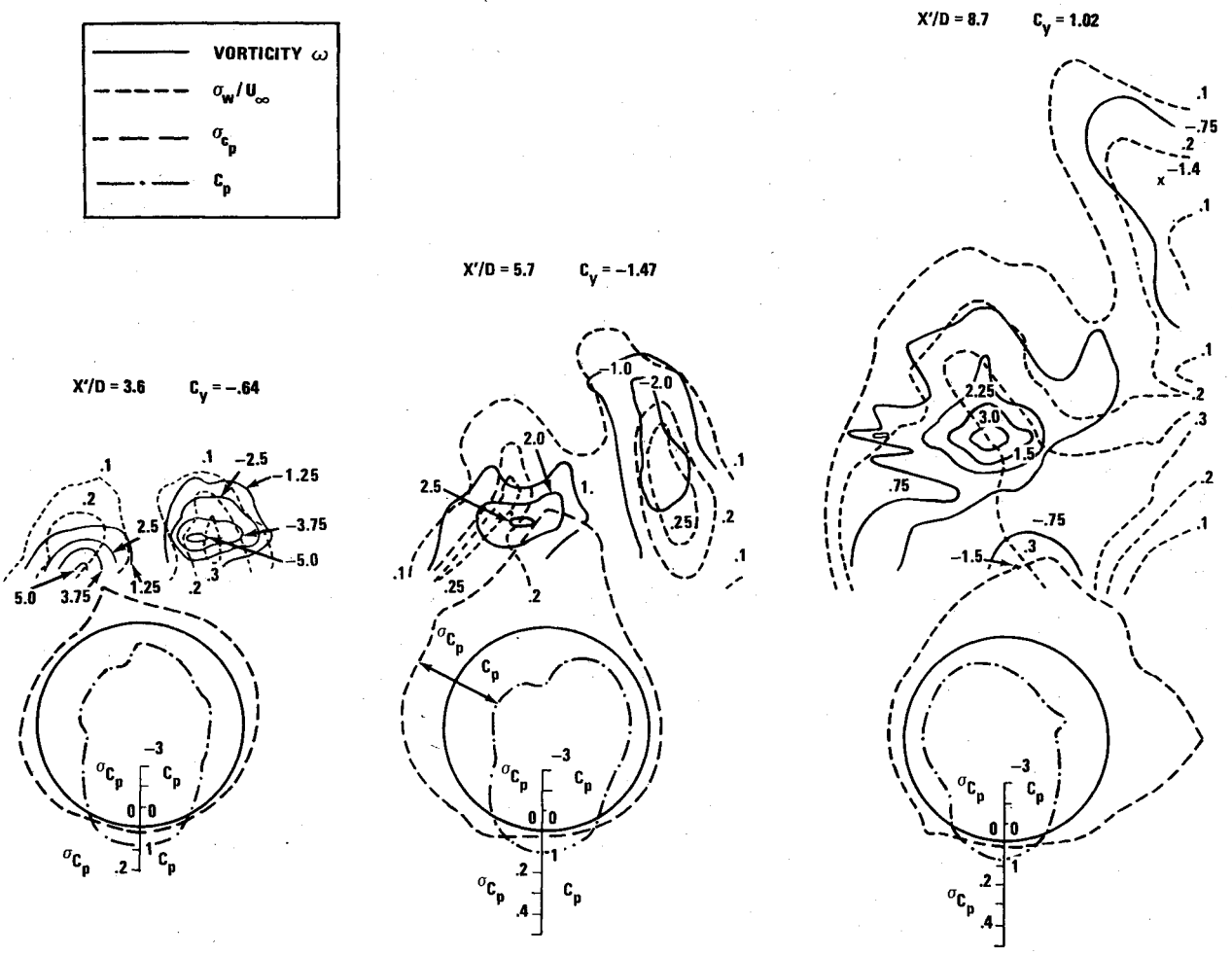

Fig. 5 Development of flowfield at incidence of 45 deg. C_p and σ_{C_p} are measured from the circular body surface with negative values appearing inside the circle.

traverse plane 3, $\alpha = 55$ deg), peak circulation values near the model surface are markedly lower and the structure of the vortex is more amorphous. The resulting pressure distribution loses much of its asymmetry and local side force coefficients become small.

The cross-sectional pressure profiles at the axial locations featuring the maximum local side force coefficient are shown in greater detail in Fig. 7. In each case the pressure levels on the side with the shed vortex and the side retaining its vortex appear to assume relatively constant values between the separation and the rear stagnation point. With increasing incidence the C_p values on the side with the remaining vortex decrease while those on the alternate side are relatively unchanged. Although the point of separation is difficult to determine from the pressure profiles, particularly at incidences of 55 deg, it appears that the separation point moves leeward on the side of the model with the closer vortex. Presumably this is caused by the rotation of this vortex toward the pitch plane at the time of vortex shedding.

The ratio of the axial velocity to $U_\infty \cos\alpha$ is shown in Fig. 8. At incidences of 55 deg values of this parameter are 0.85-2. Peaks tend to occur near vortex centers indicating a flow down the vortex cores, while minimums are located between the edge of the vortex and freestream. Parameter values are 0.85-1.15 at incidences of 25 and 35 deg.

Normal and Side Force Distributions

The local crossflow drag and side force obtained by integrating the measured pressure distributions are plotted in Fig. 9 for incidences of 45 and 55 deg. Data for each incidence were acquired in three sequential tests completed in a single day. Between tests the wind tunnel was shut down.

For the purposes of comparison with Lamont and Hunt's correlation[6] the sign of the side force shown in this figure has been adjusted to reflect a positive value on the first peak. As is shown in Fig. 9, the measured value of the side force repeats best at an incidence of 45 deg and agrees well with the correlation. At an angle of 55 deg the measured values produced in the three repeat runs are in good agreement with one another and the correlation except at the first two pressure stations. Here one of the measurements is about 20% lower than the remaining two. A detailed comparison of two pressure profiles corresponding to the high and low side force values is shown in Fig. 10. It is clear from this graph that two distinct pressure profiles occur in each of these two cases and that the difference between the profiles is generally much larger than the standard deviation of the measurement, which is indicated at each point by a vertical line. The C_p values from these two runs differ by as much as 50%. However, discrepancies on the two sides of the model tended to cancel each other to produce an integrated side force variation which is much smaller.

The least repeatable of the experimental results occurred at $\alpha = 35$ deg. Here one run produced a high side force level at pressure stations 5 and 6 which was in good agreement with the Lamont and Hunt correlation, while the remaining runs produced a very low side force level. A comparison of the high and low side force level pressure profiles (see Ref. 19) again shows that the difference between the two mean profiles is generally larger than the standard deviation of the

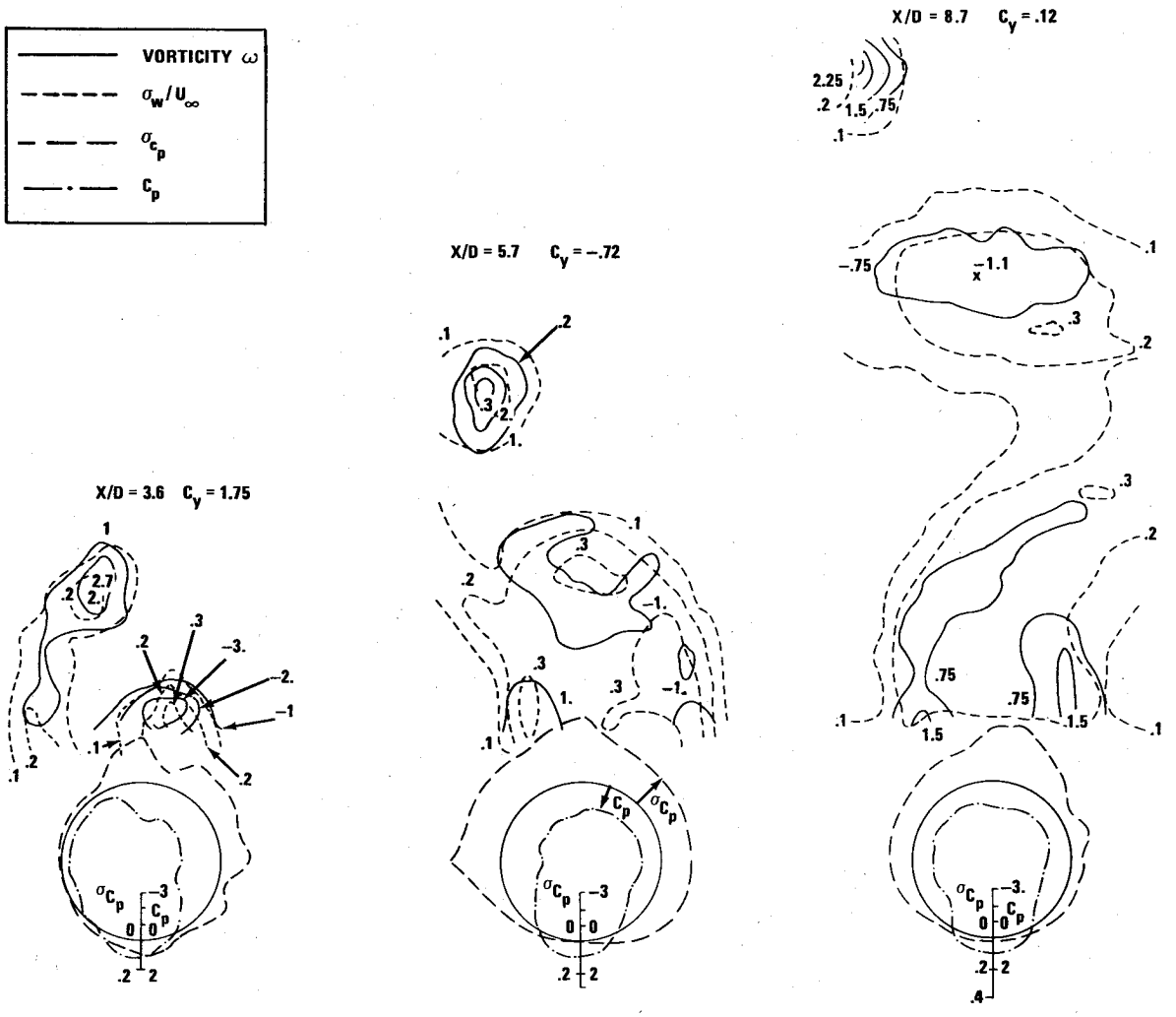

Fig. 6 Development of flowfield at incidence of 55 deg. C_p and σ_{C_p} are measured from the circular body surface with negative values appearing inside the circle.

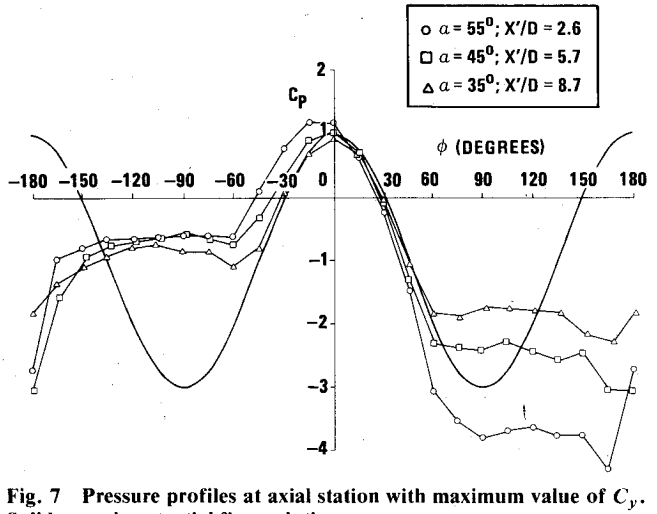

Fig. 7 Pressure profiles at axial station with maximum value of C_y. Solid curve is potential flow solution.

measurements. At an incidence of 25 deg the measured side force was very small and well below the level indicated by the Lamont-Hunt correlation. It can be seen from Fig. 9 that there is a relation between crossflow drag and local side force coefficient. Repeat runs which produced the highest side force magnitudes also yielded the largest crossflow drag coefficients.

IV. Discussion of Results

During the current tests large surface pressure and velocity fluctuations were observed downstream of the nose. The high levels of velocity fluctuation occurred in regions where the flow was separated and large pressure variations were found on surfaces adjacent to these regions. Unfortunately, the current data do not directly show whether the fluctuations are due to turbulence or to unsteadiness in the vortex pattern of which switching to the mirror image state is the extreme example. Although the boundary-layer separation is laminar, the leeward flowfield can be expected to be turbulent. Studies on yawed and unyawed cylinders indicate that the shear layer springing from the separation point changes to turbulence at $Re_c > 400$ prior to feeding into the leeward vortices.[22,23] Extrapolating the data of Ref. 23 to the current test conditions suggests that the shear layer will undergo transition as it passes the model shoulder and that most of the feeding sheet should also be turbulent.

The data presented in Sec. III appear to rule out switching of vortices to mirror image states. The velocity fluctuation contour maps (see Figs. 3, 5, and 6) indicate that very high and very low values are found on opposite sides of the survey plane. Switching to a mirror image state should induce relatively high fluctuation levels all across the flowfield. The pressure and velocity sample distributions were examined and did not exhibit sufficient bimodality to suggest the frequent occurrence of mirror image switching. The correlation between simultaneously measured surface pressures at the same circumferential angle but at alternate axial stations was

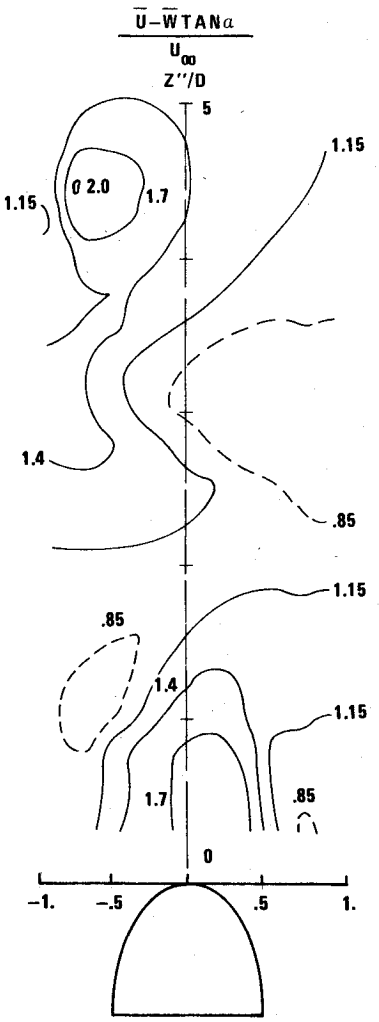

Fig. 8 Axial velocity component contours on third traverse plane at incidence of 55 deg.

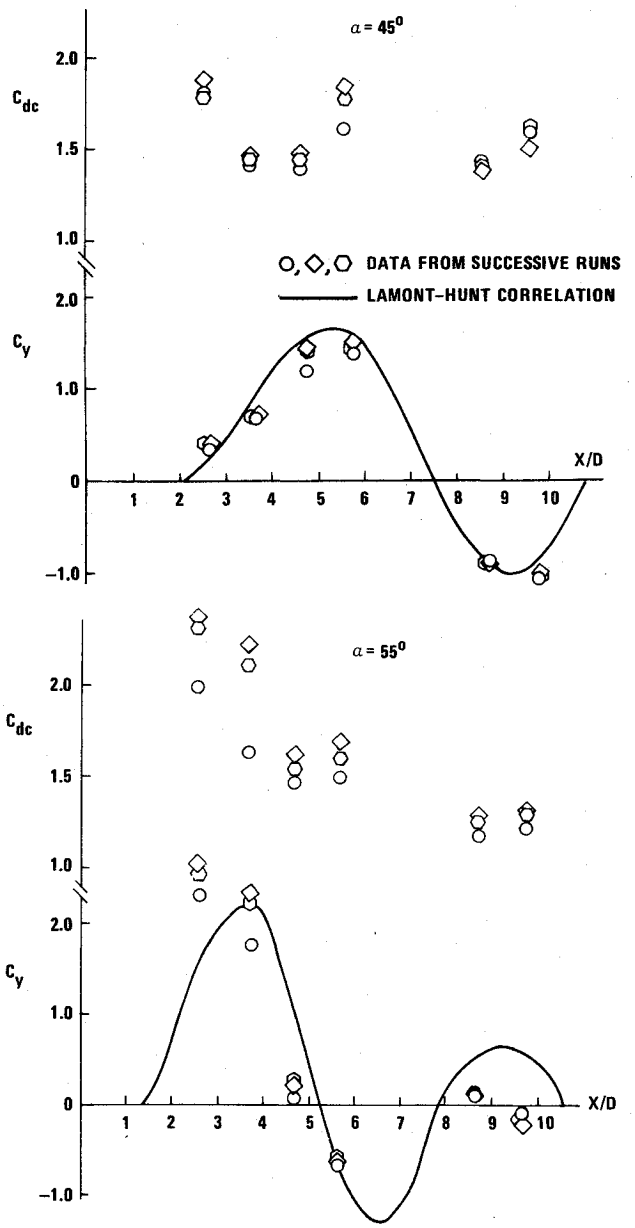

Fig. 9 Crossflow drag and side force coefficients on three repeat runs.

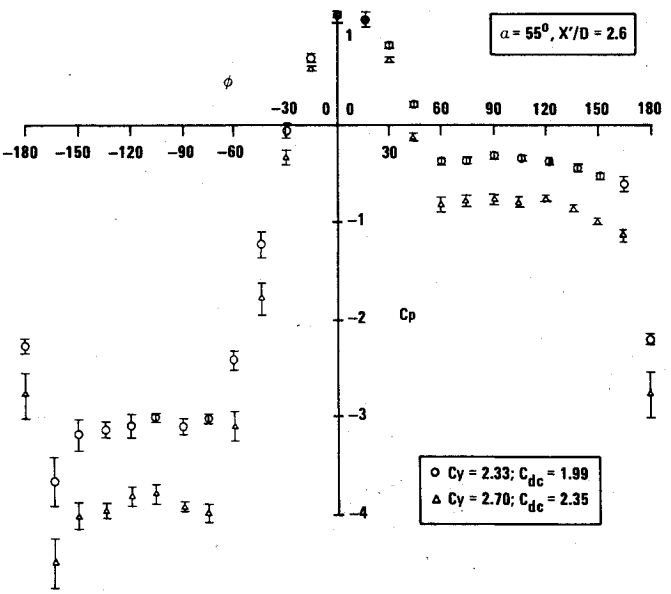

Fig. 10 Pressure profiles from two repeat runs at $\alpha = 55$ deg (vertical line represents standard deviation of measurement).

also calculated. Typical values on the leeside of the model were on the order of 0.1-0.4 for a sample of 200 points. These results suggest a coherent vortex pattern variation but appear to be too small to support the hypothesis of clearly defined vortex switching.

There is circumstantial evidence indicating that the vortex pattern is unsteady far from the model nose. As is clearly demonstrated in Figs. 5 and 6, on the foremost survey planes high-turbulence levels are confined to regions exhibiting large values of vorticity. On the aft survey plane peak vorticity values are lower and high levels of velocity fluctuation occur outside the regions of high vorticity. The extension of the region of high turbulence and lowering of peak vorticity suggests that the vortices are unsteady. High-turbulence levels are induced outside the indicated vortex position, which is its average location, by vortex motion. Similarly, the lowered vorticity peaks, which are also average values, reflect the fraction of time that the vortex is away from its mean position. An examination of the flowfield near the axial station exhibiting peak side force suggests that the vortex pattern is predominantly steady.

As was previously discussed, side force values and surface pressure profiles did not always show a high degree of repeatability. During the present study nonrepeatability appears attributable to changes in the mean vortex pattern. Pressure profiles are exhibited in Fig. 10 for repeat runs which did not accurately reproduce side force. The influence of unsteadiness appears small since the standard deviation of the pressure measurements is typically less than the difference between the two pressure profiles producing the varying side force levels.

V. Summary and Conclusions

Low-speed wind-tunnel tests have been carried out on a rigidly mounted tangent ogive model at incidences of 25, 35, 45, and 55 deg. The measured freestream turbulence level was 0.1% and a constant crossflow Reynolds number of 1×10^5 was maintained throughout the study which produced a laminar boundary-layer separation.

Flowfield velocities were measured using a three-component LDV system and unsteady surface pressure measurements were recorded using internally mounted scanivalves and transducers. At each point in the flowfield and on the model surface 200 samples were recorded, allowing means and standard deviations of velocities and pressures to be calculated. An analysis of the collected data leads to the following conclusions:

1) Large velocity fluctuations occur throughout regions in which high levels of vorticity are present.

2) High levels of surface pressure fluctuation are found on the leeside of the model downstream from the nose. Surfaces experiencing large pressure variations are generally adjacent to portions of the flowfield in which large velocity fluctuations occur.

3) The maximum side force is generated as the first vortex is shed into the flowfield and is directed toward the side with the remaining vortex. This force is a result of the large suction induced on the model by the remaining vortex.

4) The portion of the flowfield causing peak side force is predominantly steady during this study and nonrepeatability appears to be a product of changes in the mean vortex pattern.

5) In repeat runs where side force did not accurately reproduce, higher values were accompanied by larger crossflow drag coefficients.

6) Far from the nose the flowfield measurements show a decrease in peak vorticity and vortex structures appear more amorphous. This is accompanied by the disappearance of a highly asymmetric pressure distribution and large local side force levels.

7) Large-scale velocity and pressure fluctuations do not appear to be caused by a single mechanism such as vortex switching or flowfield turbulence. Although mirror image vortex switching appears to be unlikely, there is circumstantial evidence to support coherent vortex unsteadiness far from the nose.

Acknowledgments

This project was supported by William C. Volz of the Naval Air Systems Command and the Naval Sea Systems Command. The authors wish to thank Comdr. Marle Hewett and his staff at the U. S. Naval Academy for making the wind-tunnel testing facilities available. M. Szelingowski, D. Ausherman, G. Payne, and M. E. Falusi also made significant contributions to this paper.

References

[1] Clark, W. H., "Body Vortex Formation on Missiles in Incompressible Flows," AIAA Paper 77-1154, 1977.

[2] Clark, W. H. and Nelson, R. C., "Body Vortex Formation on Missiles at High Angles of Attack," AIAA Paper 76-65, 1976.

[3] Wardlaw, A. B. Jr., and Morrison, A. M., "Induced Side Forces at High Angles of Attack," *Journal of Spacecraft and Rockets,* Vol. 13, Oct. 1976, pp. 589-593.

[4] Gowens, F. E. and Perkins, E. W., "Study of the Effects of Body Shape on the Vortex Wakes of Inclined Bodies at M = 2," NACA RM A53I17, 1953.

[5] Lamont, P. J. and Hunt, B. L., "Pressure and Force Distributions on a Sharp-Nosed Circular Cylinder at Large Angles of Inclination to a Uniform Subsonic Stream," *Journal of Fluid Mechanics,* Vol. 76, No. 3, 1976, pp. 519-559.

[6] Lamont, P. J. and Hunt, B. L., "Prediction of Aerodynamic Out-of-Plane Forces on Ogive-Nosed Circular Cylinders," *Journal of Spacecraft and Rockets,* Vol. 14, Jan. 1977, pp. 38-44.

[7] Schwind, R. G. and Mullen, J., "Laser Velocimeter Measurements of Slender Body Wake Vortices," AIAA Paper 79-0302, 1979.

[8] Oberkampf, W. L., Bartel, T. J., and Martindale, W. R., "Supersonic Flow Measurements in the Body Vortex Wake of an Ogive Nose Cylinder," AIAA Paper 78-787, 1978.

[9] Oberkampf, W. L. and Bartel, T. J., "Symmetric Body Vortex Wake Characteristics in Supersonic Flow," AIAA Paper 78-1337, 1978.

[10] Mello, J. F., "Investigation of Normal Force Distribution and Wake Vortex Characteristics of Bodies of Revolution at Supersonic Speeds," *Journal of the Aerospace Sciences,* Vol. 26, 1959, pp. 155-168.

[11] Fiechter, M., "Über Wirbelsysteme an Schlanken Rotationskörpern und Ihren Einfluss auf die Aerodynamischen Beiwerte," Deutsch-Franzosisches Forschungsinstitut, Saint-Louis, Bericht 10/66, 1966.

[12] Tingley, B. E. and Allen, C. Q., "An Investigation of the Normal Force and Vortex Wake Characteristics of an Ogive-Cylinder Body at Subsonic Speeds," NASA TN D-1207, 1962.

[13] Fidler, J. E., Schwind, R. G., and Nielsen, J. N., "Investigation of Slender-Body Vortices," *AIAA Journal,* Vol. 15, Dec. 1977, pp.1736-1741.

[14] Grosche, F. R., "Wind Tunnel Investigation of the Vortex System Near an Inclined Body of Revolution With and Without Wings," *Aerodynamic Interference,* AGARD CP-71, 1971, pp. 2-1, 2-13.

[15] Thomson, K. D. and Morrison, D. F., "The Spacing, Position and Strength of Vortices in the Wake of Slender Cylindrical Bodies at Large Incidence," *Journal of Fluid Mechanics,* Vol. 50, No. 4, 1971, pp. 751-783.

[16] Yanta, W. J. and Wardlaw, A. B., "Laser Doppler Velocimeter Measurements of Leeward Flowfields on Slender Bodies at Large Angle-of-Attack," AIAA Paper 77-660, 1977.

[17] Foley, J. E., "Results of a Study of Mach Number and Reynolds Number Effects on the Lee Side Vortex Flow Field Characteristics of an Ogive-Cylinder-Frustum-Cylinder at Angles-of-Attack to 25 Degrees," Chrysler Corp., TN-AP-72-565, 1972.

[18] Owen, F. K. and Johnson, D. A.,"Wake Vortex Measurements of an Ogive Cylinder at $\alpha = 36$ Degrees," *Journal of Aircraft,* Vol. 16, Sept. 1979, pp. 577-583.

[19] Wardlaw, A. B. and Yanta, W. J., "The Flow Field About and Forces on Slender Bodies at High Incidence," AIAA Paper 80-0184, 1980.

[20] Yanta, W. J., "A Three Dimensional Laser Doppler Velocimeter (LDV) for Use in Wind Tunnels," Paper presented at International Congress on Instrumentation in Aerospace Simulation Facilities, Naval Postgraduate School, Sept. 1979.

[21] Bursnall, W. J. and Loftin, L. D. Jr., "Experimental Investigation of the Pressure Distribution about a Yawed Circular Cylinder in the Critical Reynolds Number Range," NACA TN 2463, 1951.

[22] Bloor, S., "The Transition to Turbulence in the Wake of a Circular Cylinder," *Journal of Fluid Mechanics,* Vol. 19, Pt. 2, 1964, pp. 290-304.

[23] Smith, R. A., Moon, W. T., and Kao, T. W., "Experiments on Flow About a Yawed Circular Cylinder," ASME Paper 72-FE-2, 1972.